Periodic Mesoporous Organosilicas with 1,4-Diethylenebenzene in the Mesoporous Wall: Synthesis, Characterization, and Bioadsorption Properties

ARTICLE *in* THE JOURNAL OF PHYSICAL CHEMISTRY C · JULY 2007

Impact Factor: 4.77 · DOI: 10.1021/jp071093a

5 AUTHORS, INCLUDING:

Jian Liu
Curtin University
111 PUBLICATIONS **4,968** CITATIONS
SEE PROFILE

Xin Shi
Liaoning Normal University
20 PUBLICATIONS **887** CITATIONS
SEE PROFILE

Periodic Mesoporous Organosilicas with 1,4-Diethylenebenzene in the Mesoporous Wall: Synthesis, Characterization, and Bioadsorption Properties

Congming Li, Jian Liu, Xin Shi, Jie Yang, and Qihua Yang*

State Key Laboratory of Catalysis, Dalian Institute of Chemical Physics, Chinese Academy of Sciences, 457 Zhongshan Road, Dalian 116023, China

Received: February 8, 2007; In Final Form: May 21, 2007

The 1,4-diethylenebenzene-bridged mesoporous organosilicas and bifunctional periodic mesoporous organosilicas with various amounts of 1,4-diethylenebenzene and ethane bridging groups in the mesoporous wall were synthesized by a direct cocondensation method using P123 as structure-directing agent under acidic conditions. All the materials have ordered mesostructure with uniform pore size distributions. The BET surface area and pore diameter decrease as the amounts of 1,4-diethylenebenzene in the mesoporous wall increase. The composition of the mesoporous organosilicas was characterized by FT-IR, ^{13}C cross-polarization magic-angle spinning (CP-MAS) NMR, and ^{29}Si magic-angle spinning (MAS) NMR spectroscopy. The adsorption of lysozyme (Lz) on the resultant materials was studied at different pH values. All the adsorption isotherms have successfully been correlated by the Langmuir equation. The adsorption capacity of all materials reaches the maximum around the isoelectric point of Lz. It was found that the material with mixed composition of 1,4-diethylenebenzene and ethane in the wall exhibits higher adsorption amounts than the mesoporous ethane−silica, and the difference in the adsorption amounts between the two materials decreases as the solution pH increases, suggesting that the hydrophobic and hydrogen-bonding interaction between 1,4-diethylenebenzene and Lz is stronger than that between ethane and Lz, especially at lower pH value. FT-IR spectra of the adsorbed Lz confirm that the adsorption of Lz did not lead to the denaturation of enzyme in the pH range investigated.

1. Introduction

The immobilization of enzyme onto inorganic materials has attracted much research attention in regards of the stability of enzymes under extreme conditions (at high temperature, in organic solvent, etc.) and the enzyme reusability.[1] Mesoporous silicas are promising inorganic solid matrixes for the immobilization of biomolecules due to their high surface area and ordered and tunable pore size.[2,3] The mesoporous materials with various textural structure, morphology, composition, and surface properties were employed in the enzyme immobilization.[4−8] The driving forces during the immobilization of enzyme onto the mesoporous silicas mainly include the electrostatic, hydrophobic (weak van der Waals), and hydrogen-bonding interaction. Previous studies show that the surface functionalization of mesoporous silicas is extremely important in enhancing the interactions of the protein surfaces and the mesoporous silica surfaces.[9−11]

The periodic mesoporous organosilicas (PMOs) which were prepared using bridged organosilane, $(R'O)_3Si-R-Si(OR')_3$, as precursor represent one of the significant breakthroughs in the field of mesoporous materials.[12−14] Unlike the mesoporous silica, the surface properties (hydrophilicity/hydrophobicity, interaction with guest molecules, etc.) of PMOs can be facilely adjusted through incorporation of different kinds of the organic group in the mesoporous wall.[15−32] Moreover, the bifunctional PMOs (composed of either bridging organic units in the mesoporous wall and terminal organic groups protruding into the pore channel or various kinds of bridging organic units in the mesoporous wall) provide possibilities to obtain mesoporous materials with versatile surface properties.[23,24,33,34] The PMOs with organic group as an integrated part of the mesoporous wall may act as a unique host material for enzyme immobilization. However, only the adsorption behavior of the mesoporous ethane−silicas was investigated and compared with that of the mesoporous silica.[35,36] The author found that the enzyme (lysozyme, cytochrome *c*) adsorption capacity of the mesoporous ethane−silica was lower than that of pure mesoporous silica and the electrostatic interaction is more dominant than the hydrophobic interaction in the bioadsorption of protein, probably due to the relatively weak interaction between the enzyme molecule and $-CH_2CH_2-$ in the mesoporous wall of PMOs.

To investigate the enzyme adsorption behavior of PMOs with different composition in the mesoporous wall is important in view of both the fundamental studies and the practical applications. In this paper, we report the synthesis of 1,4-diethylenebenzene-bridged mesoporous organosilicas and bifunctional PMOs with various amounts of 1,4-diethylenebenzene and ethane bridging groups in the mesoporous wall, and the lysozyme adsorption behavior of these materials was compared. The results of Lz adsorption indicate that 1,4-diethylenebenzene has stronger interactions with lysozyme than ethane.

2. Experimental Section

2.1. Chemicals and Reagents. All reagents were analytical grade and used as purchased without further purification. 1,4-Bis(trimethoxysilylethyl)benzene (BTSEB), 1,2-bis(trimethoxysilyl)ethane (BTME), and triblock copolymer poly(ethyleneoxide)−poly(propyleneoxide)−poly(ethyleneoxide) block copolymer

* Corresponding author. Fax: +86-411-84694447. Tel.: +86-411-84379219. E-mail: yangqh@dicp.ac.cn.

10.1021/jp071093a CCC: $37.00
Published on Web 07/04/2007

$((EO)_{20}(PO)_{70}(EO)_{20}$, Pluronic 123; MW, 5800) were purchased from Sigma-Aldrich Company, Ltd. (U.S.A.). Other reagents were purchased from Shanghai Chemical Reagents. Inc., of the Chinese Medicine Group.

2.2. Synthesis of Mesoporous Organosilicas with Different Fractions of 1,4-Diethylenebenzene in the Mesoporous Wall. In a typical synthesis, 0.45 g of P123 and 2.18 g of KCl were dissolved in 11.24 g of HCl (2 M) and deionized water (2.34 g) at 40 °C under vigorous stirring. A pre-prepared mixture (4.4 mmol) of BTME and BTSEB was then added to the above solution. After stirring at 40 °C for 20 h, the reaction mixture was transferred into a Teflon-lined autoclave and aged at 100 °C under static condition for 24 h. The white precipitate was recovered by filtration and dried at room temperature. The template was extracted by refluxing 0.5 g of as-synthesized materials in 100 mL of ethanol for 24 h. The extracted mesoporous materials were denoted as BB*n*, where *n* (*n* = 0, 30, 50, 70) is the mol % of BTSEB/(BTSEB + BTME) in the initial sol mixture. BB100 was synthesized under the similar conditions as BB*n* (*n* = 0, 30, 50, 70) except that BTSEB was used as the only precursor and 0.14 g of 1,3,5-trimethylbenzene (TMB) was used during the synthesis.

2.3. Lysozyme Adsorption. A series of standard lysozyme (Lz) solutions with concentrations ranging from 0.20 to 3 mg mL^{-1} were prepared by dissolving different amounts of Lz in 100 mL of buffer solutions (pH = 6.96, potassium phosphate buffer; pH = 9.60, sodium carbonate−sodium bicarbonate buffer; pH = 11.4, sodium phosphate−sodium hydroxide buffer). A low buffer solution concentration (10 mM) was used to reduce the effect of ionic strength on the adsorption. In each adsorption experiment, 20 mg of mesoporous organosilica was suspended in 4 mL of Lz solution with different concentration. The resulting mixture was continuously shaken in a shaking bath at 293 K until equilibrium was reached (about 20 h). The supernatant was separated from the solid materials by centrifugation and filtration. The Lz content of the supernatant was measured using UV adsorption at 280 nm. The amount of Lz adsorbed was calculated by the difference of the Lz concentration before and after adsorption according to the following equation:

$$q = V_0(C_0 - C)/W$$

where q is the equilibrium adsorbed amount of the mesoporous materials, C_0 and C are the Lz concentrations at initial and equilibrium solutions, respectively, V_0 is the volume of the initial Lz solution, and W is the weight of the adsorbent.

2.4. Characterization. X-ray powder diffraction (XRD) patterns were recorded on a Rigaku RINT D/Max 2500 powder diffraction system using Cu Kα radiation (40 kV and 30 mA). The nitrogen sorption experiments were performed at 77 K on an ASAP 2000 system in static measurement mode. Prior to the measurements, the samples were outgassed at 373 K for 4 h. The pore size distribution curves were calculated from the adsorption branches of the isotherms using the Barrett−Joyner−Halenda (BJH) method. Scanning electron microscopy (SEM) images were obtained on a Quanta 200F microscope. Transmission electron microscopy (TEM) was performed on a JEM-2010 at an acceleration voltage of 120 kV. FT-IR spectra were recorded on a Thermo Nicolet Nexus 470 FT-IR spectrometer using KBr pellets. Solid-state ^{13}C (100.5 MHz) cross-polarization magic-angle spinning (CP-MAS) NMR and ^{29}Si (79.4 MHz) magic-angle spinning (MAS) NMR spectra were obtained on a Bruker DRX-400 spectrometer with the following experimental parameters: for ^{13}C CP-MAS NMR experiments, 8 kHz spin rate, 3 s pulse delay, 4 min contact time, 1000 scans; tetramethylsilane was used as a reference.

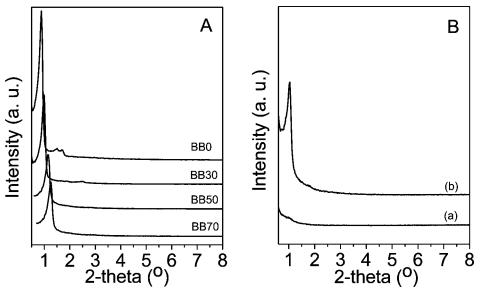

Figure 1. XRD patterns of (A) BB*n* (*n* = 0, 30, 50, 70) and (B) BB100: (a) synthesized without the addition of 1,3,5-trimethylbenzene (TMB); (b) synthesized with the addition of TMB.

3. Results and Discussion

3.1. Structural Characterization of Mesoporous Organosilicas with Different Fractions of 1,4-Diethylenebenzene in the Mesoporous Wall. The recent development of the PMOs has led to great interests in materials science. However, the synthesis of PMOs with a large and flexible organic bridging group in the mesoporous wall still remains a challenge.[37] Previously, we tried to synthesize the PMOs with 1,4-diethylenebenzene in the mesoporous wall by cocondensation of BTSEB and tetramethoxysilane (TMOS).[38] However, we found that the resultant material has low surface area (432−221 m^2/g) and pore volume (0.45−0.23 cm^3/g) because of the significant difference in the hydrolysis and condensation rate between TMOS and BTSEB. Here we choose BTME instead of TMOS considering the more compatible hydrolysis and condensation rate between BTME and BTSEB.

The X-ray diffraction patterns of BB*n* (*n* = 0, 30, 50, 70, 100) are shown in Figure 1. Three well-resolved reflection peaks in the low-angle range are observed in the XRD patterns of BB0 and BB30, which could be indexed to (100), (110), and (200) reflections of a hexagonal symmetry lattice (*p*6*mm*). This result indicates that BB0 and BB30 have highly ordered mesoporous structure. The TEM image of BB30 clearly shows the two-dimensional hexagonal arrangement of the mesopore throughout the sample, further confirming the XRD results (Figure 2A). BB*n* (*n* = 50, 70) samples synthesized with higher concentration of BTSEB exhibit one sharp diffraction peak in the low-angle region in their XRD patterns. The mesostructure of these two samples was further characterized using the TEM technique. Similar to the TEM image of BB30, the two-dimensional hexagonal arrangement of the mesopore was clearly observed in the TEM images of BB50 and BB70, which demonstrate that BB50 and BB70 have ordered hexagonal symmetry (*p*6*mm*). With the concentration of BTSEB increasing, the first diffraction peak shifts to a lower angle region, suggesting the contraction of the unit cell. The similar tendency was also observed from our previous studies.[38,39]

BTSEB has a long and flexible organic group bridged between two silicons. Therefore, it is difficult to synthesize highly ordered mesoporous organosilicas from 100% BTSEB. Previously, Burleigh et al. tried to synthesize PMOs from 100% BTSEB using cetyltrimethylammonium chloride (CTAC) as a structure-directing agent under basic conditions; however, only amorphous material was obtained.[40] In order to obtain mesoporous materials from 100% BTSEB, KCl was added in the synthetic mixture to enhance the $S^0H^+X^-I^+$ interaction between the silicate species and the hydrophilic headgroups of the nonionic surfactant and thereby to improve the mesostructure

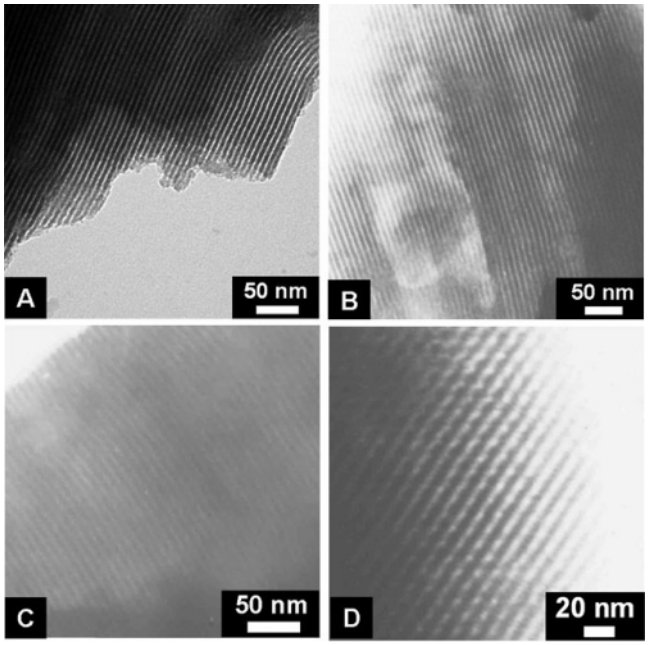

Figure 2. TEM image of BB*n*: (A) BB30; (B) BB50; (C) BB70; (D) BB100.

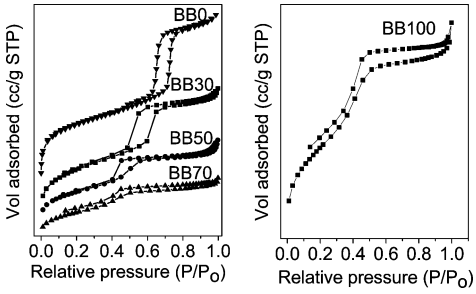

Figure 3. Nitrogen adsorption−desorption isotherms of BB*n* ($n = 0$, 30, 50, 70, 100).

order of the material. This strategy works well for the synthesis of BB*n* ($n = 0$, 30, 50, 70). However, no mesoporous material could be obtained using 100% BTSEB as the silane source as evidenced by the fact that no diffraction peaks could be observed in the XRD pattern of the material (Figure 1B). This is probably due to the fast hydrolysis and condensation rate of BTSEB. The hydrolysis and condensation rate may be a crucial step for the synthesis of mesoporous material from 100% BTSEB. 1,3,5-Trimethylbenzene is immiscible in water and is one of the most often used organic additives for the synthesis of mesoporous materials with various kinds of pore structure and morphology.[17] Furthermore, BTSEB can be well dissolved in TMB and also there are $\pi-\pi$ interactions between BTSEB and TMB. Therefore, TMB was employed with an aim to slow down the hydrolysis and condensation rate of BTSEB. The XRD pattern of BB100 (synthesized with the addition of TMB) clearly shows one sharp diffraction peak in the low-angle range, suggesting that this material has mesoporous structure (Figure 1 B). It is noteworthy to mention that the ordered alignment of mesopores in a *p6mm* symmetry can also be clearly observed in the TEM image of BB100, confirming that BB100 has ordered hexagonal mesostructure.

Figure 3 shows the N_2 adsorption−desorption isotherms of BB*n* ($n = 0$, 30, 50, 70, 100). The N_2 sorption isotherms for all materials are of type IV with a sharp capillary condensation step at relative pressure of $P/P_0 = 0.3-0.6$, which is characteristic of mesoporous materials with uniform pore size distribu-

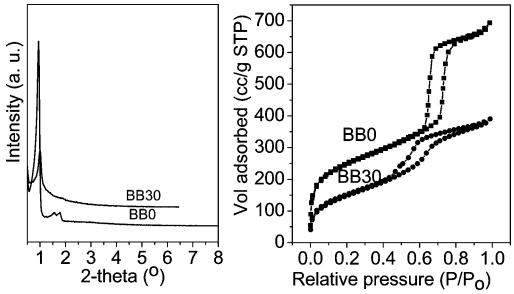

Figure 4. XRD patterns and nitrogen adsorption−desorption isotherms of BB0 and BB30 after treatment in a buffer solution at pH value of 11.4.

TABLE 1: Physicochemical Data for BB*n* ($n = 0$, 30, 50, 70, 100)

sample	*d* spacing (nm)	BET surface area (m^2/g)	pore vol (cm^3/g)[a]	pore diameter (nm)	wall thickness (nm)[b]
BB0	10.0	714	0.90	7.3	4.25
BB30	9.0	654	0.68	5.5	4.89
BB50	7.7	422	0.47	4.0	4.89
BB70	7.2	346	0.34	3.6	4.71
BB100	8.6	222	0.23	3.3	6.63
BB0[c]	9.4	872	1.07	7.27	3.58
BB30[c]	8.9	539	0.60	5.1	5.18

[a] Total pore volume obtained from the volume of N_2 adsorbed at $P/P_0 = 0.99$. [b] Wall thickness = a_0 − pore diameter, $a_0 = 2d_{100}/\sqrt{3}$. [c] BB0 and BB30 after treatment in a buffer solution at pH value of 11.4.

tions. The capillary condensation step shifts to lower P/P_0 values with increasing concentration of BTSEB in the initial sol mixture, suggesting the gradual decreasing of the pore diameter from BB0 to BB100. The BET specific surface area, pore volume, and pore diameter of BB*n* decrease in the following order: BB0 > BB30 > BB50 > BB70 > BB100 (Table 1). It is worthy to mention that all materials synthesized with different fractions of BTSEB have ordered mesoporous structure with uniform pore size distributions. The BET surface area and pore volume of BB30 and BB70 are much larger than their counterparts synthesized from TMOS and BTSEB,[38] suggesting that the hydrolysis and condensation rates of BTME and BTSEB are more compatible than that of TMOS and BTSEB.

The stability of mesoporous materials in basic medium is very important for their practical application. The stability of BB0 and BB30 in basic medium was investigated. The XRD patterns and N_2 adsorption isotherms of BB0 and BB30 after treatment in a buffer solution at a pH value of 11.4 for 20 h are displayed in Figure 4. BB0 and BB30 after treatment almost exhibit similar XRD patterns to that before treatment, which indicates that the mesostructure of BB0 and BB30 is very stable under basic medium. The N_2 sorption isotherms for BB0 and BB30 after treatment are of type IV with a sharp capillary condensation step, which is characteristic of mesoporous materials with uniform pore size distributions. In comparison with untreated samples, the BET surface area, pore diameter, and pore volume of BB0 and BB30 after treatment change slightly (Table 1). The combined results of the XRD and the N_2 sorption isotherm indicate that the mesostructure of BB0 and BB30 is stable enough to survive the treatment process under basic medium. The high stability of BB0 and BB30 makes it possible for them to be used in basic medium.

The SEM images of BB*n* are presented in Figure 5. For samples BB*n* ($n = 0$, 30, 50), ropelike macrostructure with lengths extended to several hundred micrometers and diameters

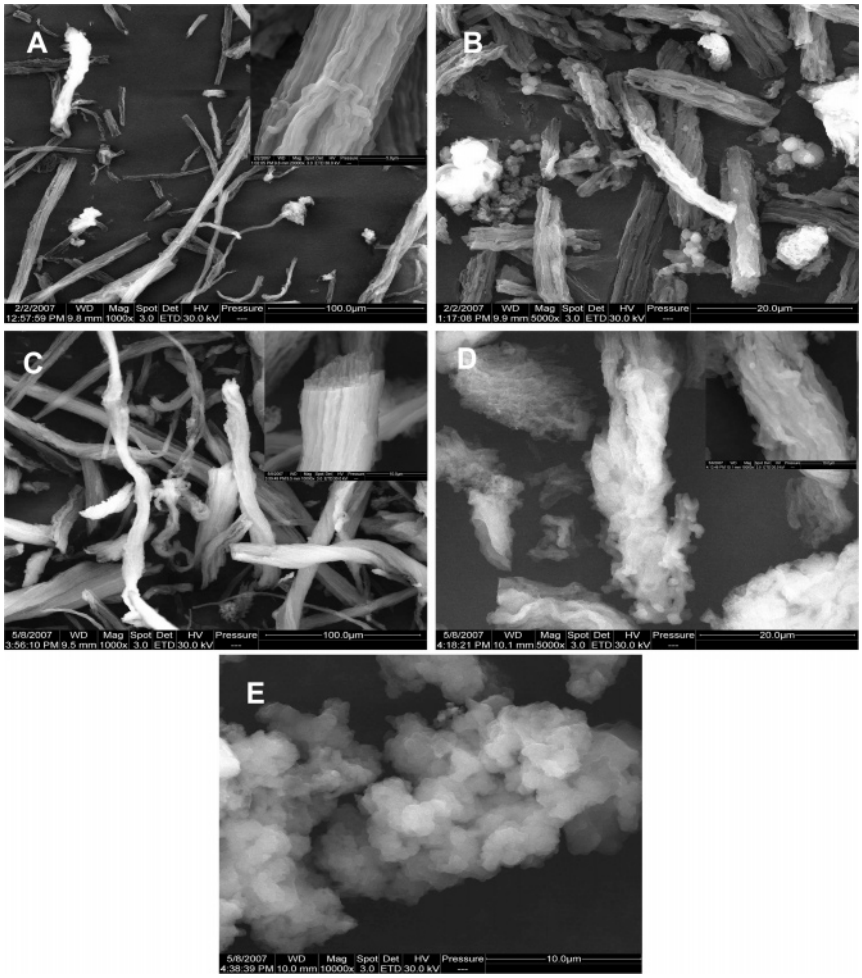

Figure 5. SEM images of BB*n*: (A) BB0; (B) BB30; (C) BB50; (D) BB70; (E) BB100.

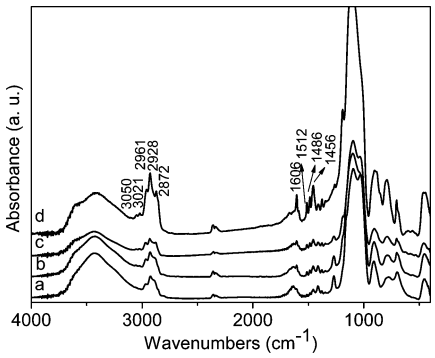

Figure 6. FT-IR spectra of BB*n*: (a) BB30; (b) BB50; (c) BB70; (d) BB100.

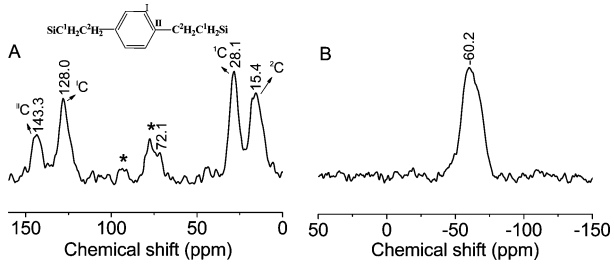

Figure 7. (A) ^{13}C CP-MAS NMR and (B) ^{29}Si MAS NMR spectra of BB100. Asterisks denotes the spinning sidebands.

of ∼10 μm are predominant. At a higher magnification, it can be seen that these ropelike particles are actually composed of long fibers with the longitude axis parallel to that of the "ropes". With the content of BTSEB increasing, for sample BB70, the aspect ratio of these "ropes" decrease substantially and the fibers become shorter and more curved. For sample BB100 synthesized with 100% BTSEB with the aid of TMB, no ropelike morphology can be observed. Instead, irregular large particles composed with small spherical aggregates are predominant.

3.2. Composition Information. FT-IR spectra of BB*n* were presented in Figure 6. The vibration peaks at 2961, 2928, and 2872 cm^{-1} are assigned to the CH stretching vibrations of $-CH_2CH_2-$ and ethylene of 1,4-diethylenebenzene groups. The bands at 3021 and 3050 cm^{-1} are attributed to the CH stretching vibrations of the phenylene groups. The bands at 1606, 1512, 1486, and 1456 cm^{-1} are attributed to the C═C vibration of the aromatic ring. From BB30 to BB100, the intensity of the vibration peaks in the range of 1606−1456 cm^{-1} increases gradually, suggesting the increased concentration of 1,4-diethylenebenzene groups in the resultant materials. The weak signals at 1348 and 1377 cm^{-1} are due to the P123 surfactant residues. The intensity of these peaks is very weak, suggesting that most of the surfactant was removed by the solvent extraction method.

The composition of BB100 was further investigated by solid-state NMR spectroscopy (Figure 7). The intense signals at 128.0 and 143.3 ppm can be attributed to the aromatic carbon I and II (see Figure 7A for details), respectively.[37] The signals at 15.4 and 28.1 ppm are assigned to ^{1}C and ^{2}C carbon of $-Si^1CH_2^2-CH_2-C_6H_{4-}{}^2CH_2{}^1CH_2Si-$, respectively.[22] The weak signal at 72.1 ppm is due to the P123 surfactant residues, suggesting that

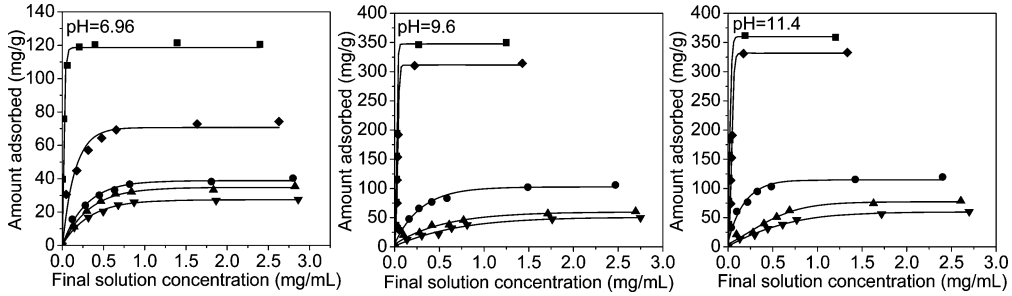

Figure 8. Adsorption isotherms of lysozyme (Lz) on BB*n* at different pH values: (■) BB30; (◆) BB0; (●) BB50; (▲) BB70; (▼) BB100.

most of the surfactant was removed by the solvent extraction process method.[41] The ^{29}Si MAS NMR spectrum of BB100 shows a signal centered at −60.2 ppm corresponding to the T site of silicon bridged between 1,4-diethylenebenzene. The absence of signals of Q^n [$Si(OSi)_n(OH)_{4-n}$] species in the range of −90 and −120 ppm indicates that all silicon atoms are covalently connected to carbon atoms and no carbon−silicon bond cleavage occurred under the present synthesis conditions. The results of FT-IR and solid-state NMR spectroscopy clearly show the existence of the organic groups in the mesoporous materials.

3.3. Lysozyme Adsorption. The immobilization of protein has attracted much attention due to its scientific importance and application in many areas. The protein hen egg white lysozyme has received special attention due to its many applications and well-understood structural characteristics.[2−4] Lysozyme has a molecular weight of about 14 000 Da and a size of 3.0 × 3.0 × 4.5 nm^3. The isoelectric point (pI) of Lz is 11.0.[42] The adsorption isotherms of Lz on BB*n* in solutions with different pH ranging from 6.96 to 11.4 are shown in Figure 8. It is found that all isotherms show a sharp initial rise and then reach maximum adsorption amounts, which suggest that these isotherms are of the Langmuir type. The solid lines in these figures represent a fit of the experimental data employing the Langmuir model.

In all pH values, the amounts of Lz adsorbed increase in the following sequence: BB30 > BB0 > BB50 > BB70 > BB100. BB30 exhibits the highest adsorption capacity among all the materials. The adsorption capacity of BB50, BB70, and BB100 is much lower compared with that of BB30 and BB0. From the results of the N_2 sorption isotherm we could know that the pore diameter of BB*n* (n = 50, 70, and 100) is less than 4.5 nm, suggesting that most Lz is adsorbed on the external surface of BB50, BB70, and BB100 due to the pore size restriction. In this case, the surface area is the key point to determine the adsorbed amounts of Lz. BB50 with higher surface area exhibits higher adsorption capacity than BB70 and BB100. BB0 has a slightly higher surface area and larger pore diameter than BB30. From the SEM images we could see that these two materials have almost the same morphology. The fact that BB30 exhibits higher adsorption capacity than BB0 should be explained by their mesoporous wall composition, suggesting that the 1,4-diethylenebenzene group in the mesoporous wall will lead to higher Lz adsorption capacity than the $-CH_2CH_2-$ group.

The maximum amounts of Lz adsorbed significantly change with the solution pH (Figure 9). Generally speaking, the Lz adsorption capacity increases with the solution pH, and the maximum adsorption capacity was observed at pH of 11.4, which is a similar tendency to previous observations.[4,43] BB30 exhibits the maximum Lz adsorption amounts of 360 mg/g at pH of 11.4. Increasing the pH from 6.96 to 9.6 results in a sharp increase of the Lz adsorption amounts. Further increasing the

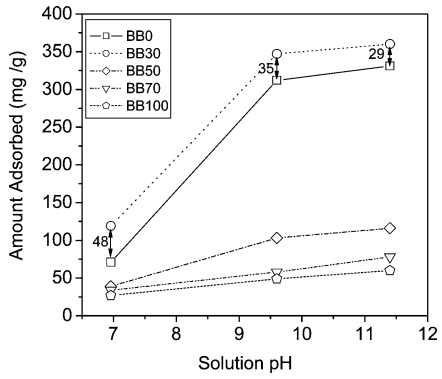

Figure 9. Maximum amounts of Lz adsorbed on BB*n* at different pH values.

pH to 11.4 only leads to slight increase of the adsorption amounts of Lz. It is believed that below the pI of Lz and above pI of the mesoporous silica (pI ≈ 2), the main driving force for the enzyme adsorption is the electrostatic interaction. The negative charge of the organosilica surface is higher at the solution pH of 9.6 than at pH of 6.96. At the same time, the net charge of Lz is very low; thus, the Lz molecules can pack closely on the adsorbent surface because of the decreased repulsion between the amino acid residues on the surface of Lz. This is the reason for the higher adsorption amounts observed at a pH of 9.6 compared with that of 6.96. Further increasing the pH to 11.4, the net charge of Lz is near zero; therefore, the electrostatic interaction between the solid material and Lz is decreased, which results in only a slight increase of the adsorbed amounts.

It is noteworthy to mention that the adsorption difference between BB30 and BB0 is 48, 35, and 29 mg/g at solution pH of 6.96, 9.6, and 11.4, respectively. This result indicates that the adsorption difference between BB30 and BB0 decreases as the solution pH increases. Previous studies show that the adsorption of enzyme on mesoporous silicas is determined by several factors under given conditions including the electrostatic interactions between the surface silanol groups and the surface charge of the amino acid residues on the surface of the enzyme, the hydrophobic interactions between the organic groups inside the wall and nonpolar side chains of the amino acids residues on the surface of enzyme, the size of the enzyme under different pH values, and repulsion between the amino acid residues on the surface of the charged enzymes, the textural properties of the solid material, etc. At a pH below the pI of enzyme, the electrostatic interaction is regarded as the main driving force for the enzyme adsorption. But the big difference in the Lz adsorbed amounts on BB30 and BB0 cannot be explained by the electrostatic interaction (the pI of BB30 and BB0 should be almost the same). Also, it cannot be only explained by the hydrophobic interaction because the difference in adsorption

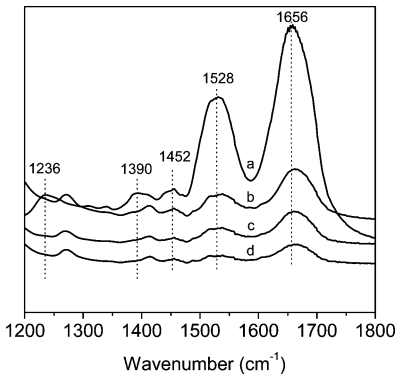

Figure 10. Comparison of the FT-IR spectra of pure lysozyme (Lz) (a) and Lz loaded on BB30 at different pH values: (b) pH = 11.4; (c) pH = 9.6; (d) pH = 6.96.

amounts between BB30 and BB0 at a pH near the pI of Lz is not as big as at a pH of 6.96. It is well-known that various kinds of C−H donors and π-acceptors situated on the surface and also in the interior of biological macromolecules can lead to the formation of C−H···A and X−H···π interactions.[44] The 1,4-diethylenebenzene group on the surface of BB30 may form a X−H···π hydrogen bond with the amino acid residues on the surface of Lz. The chances for the formation of a hydrogen bond between Lz and $-CH_2CH_2-$ is low because of the rigid structure of the ethane moiety bridged in the mesoporous wall. The existence of additional weak hydrogen-bonding interaction can explain the much higher adsorbed amounts of Lz on BB30 than on BB0 at low pH value. When the pH is near the pI of Lz, the Lz is closely packed and the chances for the formation of a hydrogen bond between the organic group on the surface of BB30 and Lz surface is decreased compared with that at low pH value. Therefore, in this case, the differences between the adsorbed amounts of Lz on BB30 and BB0 are decreased. The Lz adsorption experiment indicates that the composition of the mesoporous organosilica has great influence on the Lz adsorption behavior of these materials. The material with the 1,4-diethylenebenzene group in the mesoporous wall has a stronger interaction with Lz than that with the $-CH_2CH_2-$ group.

The structural stability of Lz on the mesoporous organosilica was checked using the FT-IR technique (Figure 10). The amide bands I−III of Lz are generally employed to study the protein structure.[4] The amide I band at 1656 cm^{-1} is due to the C═O stretching mode, whereas the amide II band (near 1528 cm^{-1}) is ascribed to the coupling of bending and the stretching modes of N−H and C−H vibrations, respectively. The amide III band (about 1236 cm^{-1}) is ascribed to the stretching and bending mode of C−N and N−H. The bands at 1452 and 1390 cm^{-1} are ascribed to the CH_2 and CH_3 stretching modes of aliphatic moieties of amino acid side chains. The FT-IR spectra of BB30 loaded with Lz at different pH solutions are displayed in Figure 10. All the BB30/Lz composites exhibit the amide bands I−III, indicating that the structural conformation of Lz is retained after adsorption onto BB30. These results confirm that the adsorption of Lz on the mesoporous organosilicas does not lead to denaturation of Lz.

4. Conclusions

The bifunctional mesoporous organosilicas with different fraction of 1,4-diethylenebenzene and ethane groups in the mesoporous wall were synthesized by the cocondensation method. The 1,4-diethylenebenzene-bridged mesoporous organosilica was also successfully synthesized with the aid of TMB for the first time. The mesoporous wall composition of the mesoporous organosilicas was fully characterized by FT-IR and the solid-state NMR technique. The enzyme adsorption properties of these mesoporous organosilicas has been studied in an Lz solution with different pH values. It has been found that the amounts of Lz adsorbed depend on the surface characteristics and the textural properties of the mesoporous organosilicas and the solution pH. The maximum Lz adsorption amount of 360 mg g^{-1} has been achieved on BB30 at a solution pH of 11.4. BB30 with a fraction of 1,4-diethylenebenzene in the mesoporous wall exhibits much higher adsorption capacity for Lz than BB0 with only the ethane moiety in the mesoporous wall. This is probably due to the fact that the 1,4-diethylenebenzene group can form stronger hydrophobic and hydrogen-bonding interactions with Lz than the $-CH_2CH_2-$ group. FT-IR spectra confirm that immobilization of Lz does not result in the denaturation of the enzyme.

Acknowledgment. The authors thank Professor Can Li for the FT-IR analyses. This work was financially supported by the National Natural Science Foundation of China (20321303) and the National Basic Research Program of China (2003CB615803, 2005CB221407).

References and Notes

(1) Klibanov, A. M. *Science* **1983**, *219*, 722.
(2) Hartmann, M. *Chem. Mater.* **2005**, *17*, 4577.
(3) Yiu, H. H. P.; Wright, P. A. *J. Mater. Chem.* **2005**, *15*, 2362.
(4) Vinu, A.; Murugesan, V.; Hartmann, M. *J. Phys. Chem. B* **2004**, *108*, 7323.
(5) Lei, J.; Fan, J.; Yu, C. Z.; Zhang, L. Y.; Jiang, S. Y.; Tu, B.; Zhao, D. Y. *Microporous Mesoporous Mater.* **2004**, *73*, 121.
(6) Fan, J.; Lei, J.; Wang, L. M.; Yu, C. Z.; Tu, B.; Zhao, D. Y. *Chem. Commun.* **2003**, 2140.
(7) Fan, J.; Yu, C.; Gao, F.; Lei, J.; Tian, B.; Wang, L.; Luo, Q.; Tu, B.; Zhou, W.; Zhao, D. *Angew. Chem., Int. Ed.* **2003**, *42*, 3146.
(8) Yang, X. Y.; Li, Z. Q.; Liu, B.; Klein-Hofmann, A.; Tian, G.; Feng, Y. F.; Ding, Y.; Su, D. S.; Xiao, F. S. *Adv. Mater.* **2006**, *18*, 410.
(9) Yiu, H. H. P.; Wright, P. A.; Botting, N. P. *J. Mol. Catal. B: Enzym.* **2001**, *15*, 81.
(10) Yiu, H. H. P.; Botting, C. H.; Botting, N. P.; Wright, P. A. *Phys. Chem. Chem. Phys.* **2001**, *3*, 2983.
(11) Maria Chong, A. S.; Zhao, X. S. *Catal. Today.* **2004**, *93*−*95*, 293.
(12) Inagaki, S.; Guan, S.; Fukushima, Y.; Ohsuna, T.; Terasaki, O. *J. Am. Chem. Soc.* **1999**, *121*, 9611.
(13) Melde, B. J.; Holland, B. T.; Blanford, C. F.; Stein, A. *Chem. Mater.* **1999**, *11*, 3302.
(14) Asefa, T.; MacLachlan, M. J.; Coombs, N.; Ozin, G. A. *Nature* **1999**, *402*, 867.
(15) Asefa, T.; MacLachlan, M. J.; Grondey, H.; Coombs, N.; Ozin, G. A. *Angew. Chem., Int. Ed.* **2000**, *39*, 1808.
(16) Matos, J. R.; Kruk, M.; Mercuri, L. P.; Jaroniec, M.; Asefa, T.; Coombs, N.; Ozin, G. A.; Kamiyama, T.; Terasaki, O. *Chem. Mater.* **2002**, *14*, 1903.
(17) Burleigh, M. C.; Markowitz, M. A.; Wong, E. M.; Lin, J. S.; Gaber, B. P. *Chem. Mater.* **2001**, *13*, 4411.
(18) Guo, W.; Park, J. Y.; Oh, M. O.; Jeong, H. W.; Cho, W. J.; Kim, I.; Ha, C. S. *Chem. Mater.* **2003**, *15*, 2295.
(19) Muth, O.; Schellbach, C.; Fröba, M. *Chem. Commun.* **2001**, 2032.
(20) Sayari, A.; Yang, Y. *Chem. Commun.* **2002**, 2582.
(21) Zhang, L.; Yang, Q.; Zhang, W. H.; Li, Y.; Yang, J.; Jiang, D.; Zhu, G.; Li, C. *J. Mater. Chem.* **2005**, *15*, 2562.
(22) Nakajima, K.; Tomita, I.; Hara, M.; Hayashi, S.; Domen, K.; Kondo, J. N. *J. Mater. Chem.* **2005**, *15*, 2362.
(23) Asefa, T.; Kruk, M.; MacLachlan, M. J.; Coombs, N.; Grondey, H.; Jaroniec, M.; Ozin, G. A. *J. Am. Chem. Soc.* **2001**, *123*, 8520.
(24) Yang, Q.; Kapoor, M. P.; Inagaki, S. *J. Am. Chem. Soc.* **2002**, *124*, 9694.
(25) Goto, Y.; Inagaki, S. *Chem. Commun.* **2002**, 2410.
(26) Bion, N.; Ferreira, P.; Valente, A.; Goncalves, I. S.; Rocha. J. *J. Mater. Chem.* **2003**, *13*, 1910.
(27) Kapoor, M. P.; Yang, Q.; Inagaki, S. *J. Am. Chem. Soc.* **2002**, *124*, 15176.
(28) Kapoor, M. P.; Yang, Q.; Inagaki, S. *Chem. Mater.* **2004**, *16*, 1209.
(29) Baleião, C.; Gigante, B.; Das, D.; Álvaro, M.; Garcia, H.; Corma, A. *Chem. Commun.* **2003**, 1860.

(30) Bao, X. Y.; Zhao, X. S.; Li, X.; Chia, P. A.; Li, J. *J. Phys. Chem. B* **2004**, *108*, 4684.
(31) Bao, X. Y.; Zhao, X. S.; Qiao, S. Z.; Bhatia, S. K. *J. Phys. Chem. B* **2004**, *108*, 16441.
(32) Olkhovyk, O.; Jaroniec, M. *J. Am. Chem. Soc.* **2005**, *127*, 60.
(33) Morell, J.; Güngerich, M.; Wolter, G.; Jiao, J.; Hunger, M.; Klar, P. J.; Fröba, M. *J. Mater. Chem.* **2006**, *16*, 2809.
(34) Burleigh, M. C.; Jayasundere, S.; Spector, M. S.; Thomas, C. W.; Markowitz, M. A.; Gaber, B. P. *Chem. Mater.* **2004**, *16*, 3.
(35) Qiao, S. Z.; Yu, C. Z.; Xing, W.; Hu, Q. H.; Djojoputro, H.; Lu, G. Q. *Chem. Mater.* **2005**, *13*, 6172.
(36) Qiao, S. Z.; Djojoputro, H.; Hu, Q. H.; Lu, G. Q. *Prog. Solid State Chem.* **2006**, *34*, 249.
(37) Hunks, W. J.; Ozin, G. A. *Chem. Mater.* **2004**, *16*, 5465.
(38) Li, C.; Yang, J.; Shi, X.; Liu, J.; Yang, Q. *Microporous Mesoporous Mater.* **2007**, *97*, 206.
(39) Jiang, D.; Gao, J.; Yang, Q.; Yang, J.; Li, C. *Chem. Mater.* **2006**, *18*, 6012.
(40) Burleigh, M. C.; Markowitz, M. A.; Spector, M. S.; Gaber, B. P. *Environ. Sci. Technol.* **2002**, *36*, 2515.
(41) Huh, S.; Wiench, J. W.; Yoo, J. C.; Pruski, M.; Lin, V. S.-Y. *Chem. Mater.* **2003**, *15*, 4247.
(42) Wilson, K. P.; Malcolm, B. A.; Matthews, B. W. *J. Biol. Chem.* **1992**, *267*, 10842.
(43) Vinu, A.; Miyahara, M.; Ariga, K. *J. Phys. Chem. B* **2005**, *109*, 6436.
(44) Desiraju, G. R.; Steiner, T. *The Weak Hydrogen Bond: In Structural Chemistry and Biology*; Oxford University Press: Oxford, 1999.